Template based analysis of amorphous and nanocrystalline materials by TEM (part II)

Krzysztof Kudłacz

Introduction

The Debye scattering formula (DSF) (Debye, 1915), which represents a total scattering approach, is gaining interest as a method often considered to be more effective than standard Retvield analyses, when it comes to the withdrawing the essential information regarding structural features of nanocrystalline materials from the corresponding powder diffraction patterns (Cervellino et al. 2010). Moreover it could be used to characterize the short range order in amorphous materials based on the model proposed by Czigany and Hultman (2010). Despite the fact that the relevance and importance of the DSF has been well known since it was published in 1915, it has not receive too much attention through most of that time. The main reason behind this phenomena should be directly addressed to the computational cost of the DSF. This is, as will be shown later, an important issue in the case of the calculations performed for the systems where the preferred orientation is taken into account, and based on the equation proposed by Hudson and Hofstader (1952) which can be treated as a special case of DSF. The rapid growth of the computational power of modern computers and the possibility of applying different numerical “tricks” however, facilitate and encourage the implementation and development of dedicated software programs.

The majority of the analysis using DSF are based on the X-ray and neutron diffraction experimental data. Here, we will focus on the application of this equation(s) in the field of transmission electron microscopy. There are two main motivations for that. The first one is related with the smaller scale of observation in electron microscopy if compared to traditional XRD. The other one refers to the availability of TEM microscope. Whereas the latter can be found in many research centers, neutron or synchrotron X-ray sources are available only in dedicated facilities. In the first paper (part I) we concentrated on the analysis and interpretation of electron powder diffraction patterns (EPDP) obtained from SAED patterns of calcium carbonate precipitates formed during carbonation of calcium hydroxide solution. Here we will focus on the modeling of calcium carbonate clusters with different type of atom arrangements, calculation of corresponding electron diffraction patterns and their comparison with experimental data.

Calculation of electron powder diffraction pattern (EPDP)

In this paper we will consider two types of electron diffraction pattern calculations. The first one applies to the clusters randomly oriented in space and is based on the Debye scattering formula (Debye 1915):

$$I(\theta) = \sum_{i=1}^{N}\sum_{j=1}^{N} f_i f_j \frac{\sin\left(4\pi\frac{\sin(\theta)}{\lambda} r_{ij}\right)}{4\pi\frac{\sin(\theta)}{\lambda} r_{ij}} \quad \text{(Equation 1)}$$

where:

I - intensity

f_i - scaterring amplitude of the i-th atom

ϑ - scattering angle (2ϑ is the Bragg angle)

λ - wavelength

r_{ij} - separation vector of i-th and j-th atoms in a cluster

The other one set of calculations applies to the clusters which show preferred orientation and is based on the equation proposed by Hudson and Hofstadter (1952):

$$I(\theta) = \sum_{i=1}^{N}\sum_{j=1}^{N} f_i f_j \cos\left[2\pi S_{ij}(1-\cos(2\theta))/\lambda\right] \; x\, J_0\left(2\pi D_{ij}\frac{\sin(2\theta)}{\lambda}\right) \quad \text{(Equation 2)}$$

where:

S_{ij} - separation vector of i-th and j-th atom in a cluster along the direction of electron beam

D_{ij} - separation vector of i-th and j-th atom projected on the plane perpendicular to the electron beam direction

J_0 - Bessel function of zero order

Note that the calculation of Bessel function (which is calculated for every of i-th and j-th atom in the cluster) significantly increases computational time. Apart from that there is a general problem of its numerical approximation. Here both approximation of Bessel function and numerical "trick" which speeds up the computation of Equation 2 are presented. First, lest us consider Bessel function of n-order (n is an integer value) written as an integral expression:

$$J_n(x) = \frac{1}{\pi}\int_0^{\pi} \cos(nt - x\sin(t))\, dt \quad \text{(Equation 3)}$$

Such an expression for numerical application can be approximated by the following summation:

$$J_n(x) \cong \frac{1}{\pi}\sum_{k=0}^{N} \cos(n(k\Delta t) - x\sin(k\Delta t)) \quad \text{(Equation 4)}$$

where Δt = π/N (higher N results in smaller Δt giving better approximation of Equation 3). In computations performed here N = 200 appears to be sufficient. Such an approximation is still numerically expensive. Therefore the following trick was applied. Instead of calculating $J_n(x)$ for every i-th and j-th atom in the cluster at a θ value according to Equation 2 (where $x = 2\pi D_{ij}\frac{\sin(2\vartheta)}{\lambda}$) we can perform a set of subsequent operations:

- Determine maximal value of Bessel function argument according to $x_{max} = \max(2\pi D_{ij} \frac{\sin(2\theta)}{\lambda})$, $x_{min} = 0$ (see Equation 2). Effectively x_{max} will be the combination of the cluster diameter (if it has a spherical shape, or its maximal size otherwise) since this is the maximal value that D_{ij} can have for any possible orientation, and maximal value of sin(2θ) within consider scattering angle range.

- Declare an array A[] of M elements. Initialize this array according to the formula: A[m] = $J_n(m*\Delta x)$ using Equation 4, where $\Delta x = (x_{max} - x_{min})/M$, and m is the array index which varies from 0 to M-1.

All presented steps are performed prior to the calculation of scattering pattern or patterns if more than one orientation is considered. From now on, every time when scattering intensity is calculated, instead of calculating $J_n(x)$ (where $x = 2\pi D_{ij} \frac{\sin(2\theta)}{\lambda}$), $J_n(x)$ is replaced by the array A[] value at index m, where m = (round)$(x / x_{max}) * (M - 1)$.

Now we should consider how the position (x, y, z) of atom within the cluster volume which is changed when different orientations are considered. The orientation between two Cartesian coordinate systems can be described using Euler angles (φ_1, □, φ_2) (Morawiec 2004). In order to transform one coordinate system into another it is necessary to perform a set of orientation transformations corresponding to each of the Euler angles according to the equation:

$$(x', y', z') = O(\phi_1, □, \phi_2)\ (x, y, z) \quad \text{(Equation 5)}$$

where:

(x, y, z) – initial coordinate system

(x', y', z') – (x, y, z) after transformation

$O(\varphi_1, □, \varphi_2)$ – transformation operator (set of orientations)

There are a few different conventions regarding the sequence and the direction of the rotations. Here, one of the most popular was used, which involves the consecutive rotations around the z, x and z axis of the coordinate system subjected to rotation at an angle φ_1, □, φ_2 respectively:

$$O(\phi_1, □, \phi_2) = O(z, \phi_2)O(x, □)O(z, \phi_1) \quad \text{(Equation 6)}$$

where $0 \le \varphi_1 < 360°$, $0 \le □ \le 180°$ and $0 \le \varphi_2 < 360°$. The angular range for each rotation allows to reach any possible orientation.

It can be seen that the first rotation (i.e., $O(z, \varphi_1)$) does not change S_{ij} and D_{ij} values (used in the equation 4.17) when the z-axis of the cluster is parallel to the electron beam. Therefore selection of the initial orientation of the cluster with its z-axis parallel to the electron beam limits the EPDP

calculation to the two consecutive rotations around the *x* and *z*-axis of the cluster at angles and φ_2 respectively. Therefore the simulation of EPDP according to Equation 2 is performed for all orientation described by the equation:

$$(x', y', z') = O(z, \beta)O(x, \alpha)(x, y, z) \quad \text{(Equation 7)}$$

where:

(x, y, z) – initial cluster coordinate system with its z-axis parallel to the electron beam

(x', y', z') – (x, y, z) after transformation

$O(x, \alpha)$ – orientation around the cluster x-axis at α angle ($0 \leq \alpha \leq 180°$)

$O(z, \beta)$ – orientation around the cluster z-axis at β angle ($0 \leq \beta < 360°$)

Results

As shown in the previous paper, the estimated FWHM of the first EPDP peak corresponds to a cluster size ~10 Å. Based on that, the shape of the clusters was assumed to be a sphere of 10 Å in diameter. Four different arrangements of atoms within the cluster volume were considered. They correspond to vaterite, aragonite, calcite and monohydrocalcite. Two sets of simulations were performed, corresponding to the case of a randomly oriented clusters, as well as to the case where a possible preferred orientation develops. As we could see in the previous paper (part I), the initial amorphous structure was pseudomorphically replaced by highly oriented calcite, what could be explained by an oriented aggregation of pre-nucleation clusters which appearance preceded the formation of calcite with a well developed texture. Therefore, the equation, taking into account the development of a preferred cluster orientation is also tested (Equation 2)

The results of the simulation for randomly oriented clusters (Equation 1) and their comparison with experimental results (i.e., electron powder diffraction patterns - EPDPs) are presented in Figure 1. Calculated EPDPs corresponding to clusters with vaterite, aragonite and calcite structure (Figure 1a,b and c) do not show a good matching with experimental EPDPs (Figure 1d). The positions of the first and second peak (at ~0.34 $Å^{-1}$ and ~0.5 $Å^{-1}$ respectively) of simulated EPDP for a cluster with monohydrocalcite structure (Figure 1d) match the positions of the two first peaks of experimental EPDPs (Figure 1e).

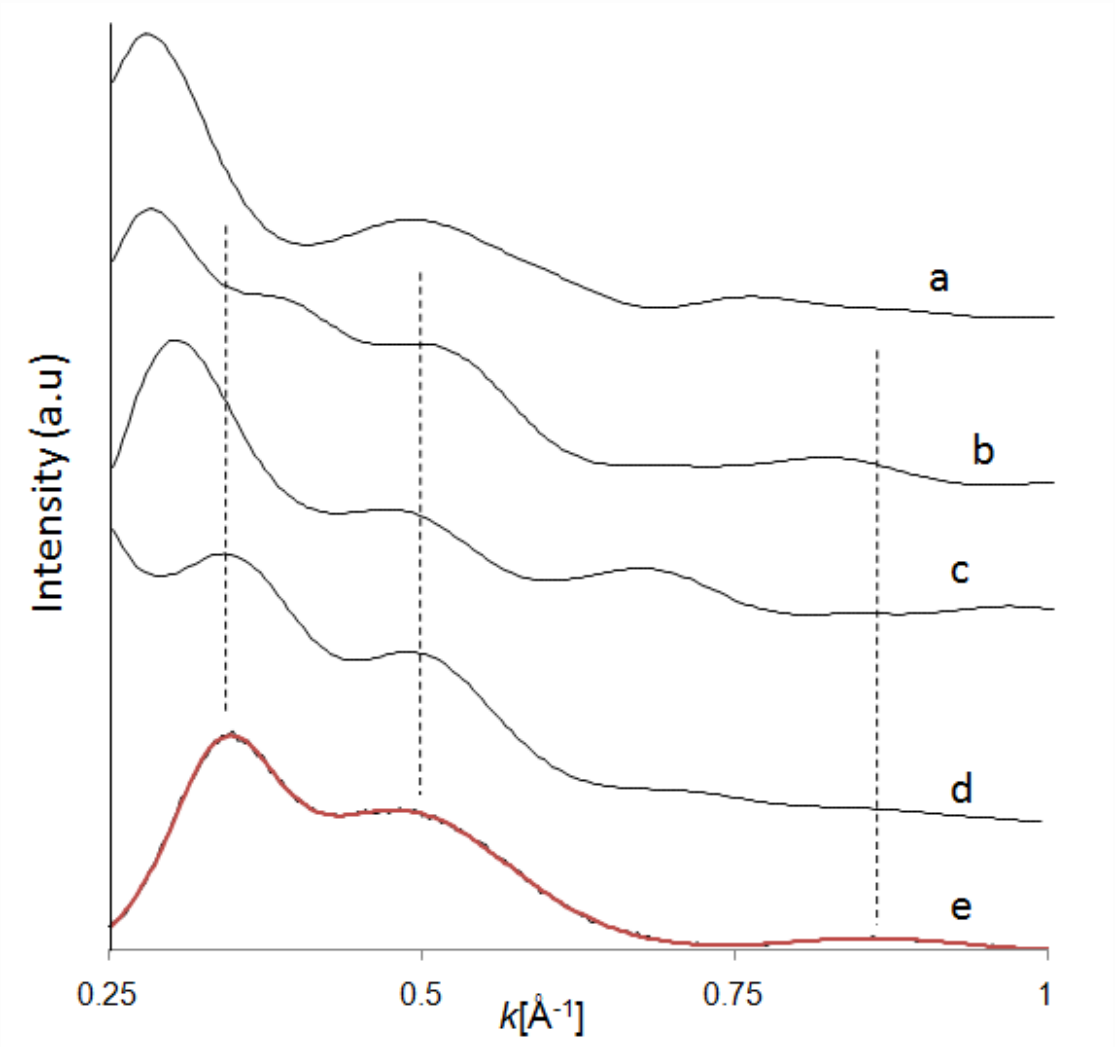

Figure 1. Comparison between simulated EPDPs for clusters with ~10 Å crystallite size and different internal structures: vaterite (a), aragonite (b), calcite (c), monohydrocalcite (d) and experimental EPDPs corresponding to ACC formed in lime water after 2 min air exposure (e) (back line: EPDP, red line: fitted function).

In order to calculate different orientations of the cluster according to Equation 2, its lattice (which is non-Cartesian in each case) has to be associated with a Cartesian coordinate system. The applied relationship between lattice vectors (**a**, **b**, **c**) of the considered structure and Cartesian axes (***x***, ***y***, ***z***) is the following: i) vaterite: **a**//***x*** and **c**//***z*** ii) aragonite **a**//***x***, **b**//***y*** and **c**//***z*** iii) calcite: **a**//***x*** and **c**//***z*** iv) monohydrocalcite: **a**//***x*** and **c**//***z***.

The procedure for EPDP simulation was the following. Initially the structure (i.e., vaterite, aragonite or calcite) was oriented with its z-axis parallel to the electron beam. Subsequently, the structure was oriented in space according to Equation 7, where α and β were changed every 5°. Finally, the cluster

shape (sphere with 10 Å in diameter) was "cut" from the oriented structure and the EPDP was simulated according to the equation 4.17. The theoretical (calculated) EPDPs were compared with experimental data (EPDPs obtained by the integration of SAED pattern-see part I) according to the equation:

$$R = \sqrt[2]{\sum_{i=1}^{n}(S(k_i) - E(k_i))^2} \quad \text{(Equation 8)}$$

where:

R – matching coefficient between calculated (from Equation 2) and profile fitted to experimental EPDPs

S – simulated EPDP intensity at k_i (wavelength) point

E – experimental EPDP intensity at k_i point

Figure 2 presents simulated EPDPs with the best matching to experimental EPDPs (i.e., with the smallest R value) for the considered types of internal structure. From all three considered types of internal structure of the cluster the best matching was obtained for clusters with calcite (Figure 2c) and monohydrocalcite (Figure 2d) structure. Their orientations correspond to $[\bar{4}\bar{2}1]$ and $[1\bar{1}0]$ zone axis parallel to the electron beam direction for clusters with calcite and monohydrocalcite structure respectively. Both calculated EPDPs show peaks at very similar positions to experimental EPDPs. This second type of simulation shows that clusters may have a preferred orientation, because, the previous simulation showing non-oriented clusters never achieved such a good matching between simulated and experimental results.

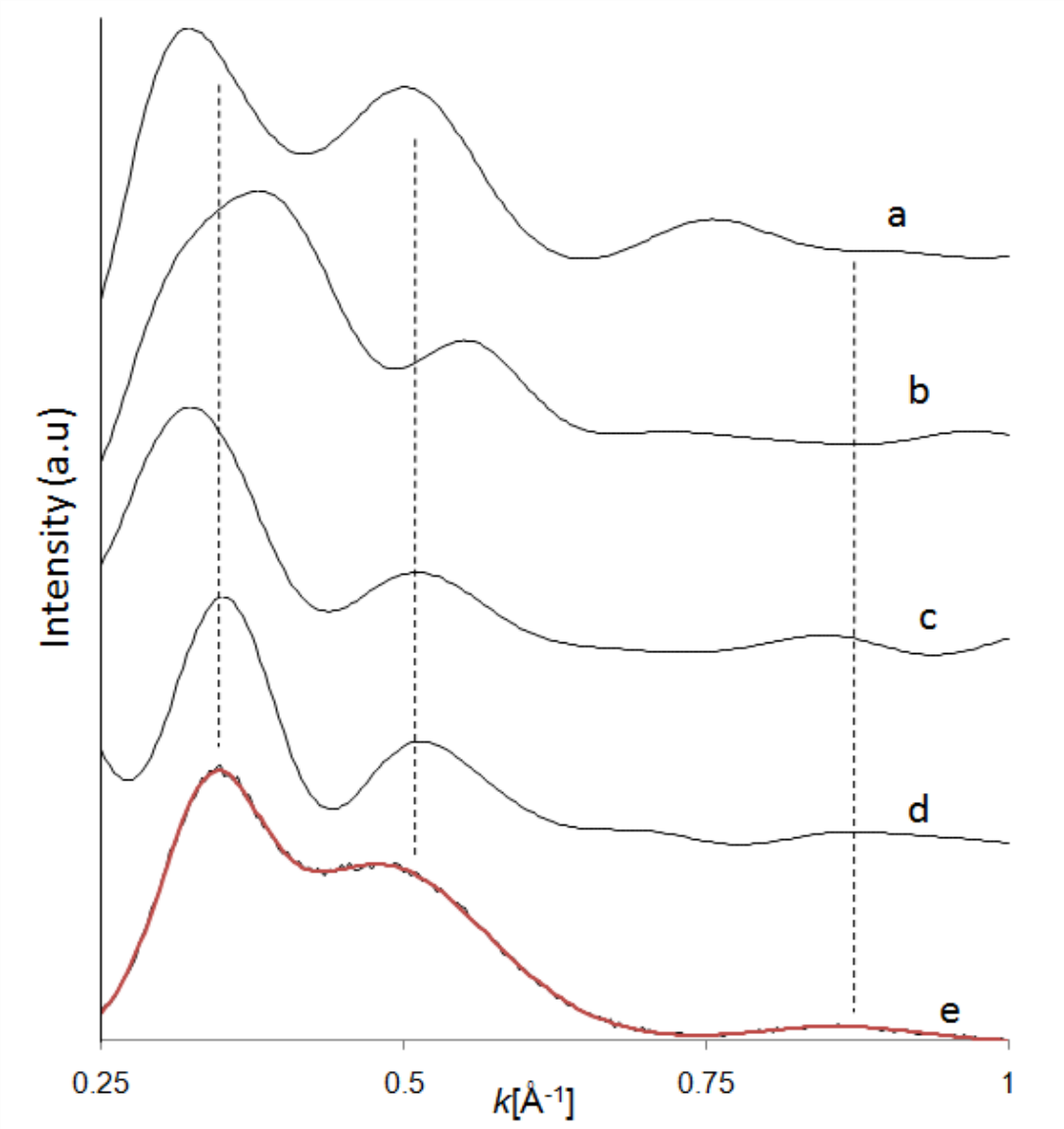

Figure 2. Simulated EPDPs for clusters (with spherical shape and 10 Å in diameter) with internal structure of vaterite (a), aragonite (b), calcite (c) and monohydrocalcite (d) displaying a preferred cluster orientation, in comparison with experimental EPDPs of ACC formed in lime water after 2 min air exposure (e) (back line: EPDP, red line: fitted function).

Conclusions

Theoretical findings combined with experimental data point to the existence of short range order in ACC with characteristics of monohydrocalcite and/or calcite. However, the reliability of simulated data may be questionable. It has to be taken into account that theoretical considerations are based on two assumptions: equal size distribution and lack of misorientation among aggregating clusters. The fact that ACC always transformed directly into calcite indicates that the observed short range

order may have an important role in crystalline phase selection. Its origin could be related to the formation of stable pre-nucleation clusters with a proto-calcite structure (short-range order) which forms ACC spheres, and transforms into calcite following an oriented aggregation (Gebauer et al. 2010). Approach to the problem of characterization of amorphous and nanocrystalline phases presented here may be easy applied in case of different materials. In general, the arrangement of atoms within cluster volume of arbitrary shape, not necessary has to be derived from predefined crystal structure, but maybe initialize by Monte Carlo methods.

References

Cervellino, A., Giannini, C and Guagliardi, A. (2010) DEBUSSY: A Debye user system for nanocrystalline materials. Journal of Applied Crystallography, 43, 1543-1547.

Czigany, Z. and Hultman, L. (2010) Interpretation of electron diffraction patterns from amorphous and fullerene-like carbon allotropes. Ultramicroscopy 110, 815-819.

Debye, P. (1915) Zerstreuung von Röntgenstrahlen. Annalen der Physik 35, 809-817

Gebauer, D., Gunawidjaja, P. N., Ko, J. Y., Bacsik, Z., Aziz, B., Liu, L., et al. (2010) Proto-calcite and proto-vaterite in amorphous calcium carbonates. Angewandte Chemie International Edition 49, 8889-8891.

Hudson, A. and Hofstadter R. (1952) Electron Diffraction from Small Crystals. Physical Review 88, 596-599.

Morawiec, A. (2004) Orientations and Rotations: Computations in Crystallographic Textures. Springer.